Available online at www.sciencedirect.com
SCIENCE DIRECT®
International Journal of Heat and Mass Transfer 47 (2004) 2795–2806
International Journal of HEAT and MASS TRANSFER
www.elsevier.com/locate/ijhmt

Heat transfer under a precessing jet: effects of unsteady jet impingement

S. Göppert [a], T. Gürtler [a], H. Mocikat [b], H. Herwig [b,*]

[a] Technische Thermodynamik, TU Chemnitz, D-09107 Chemnitz, Germany
[b] Arbeitsbereich Technische Thermodynamik (6-08), Technische Universität Hamburg-Harburg, Denickestrasse 15, D-21073 Hamburg, Germany

Received 25 February 2003; received in revised form 15 October 2003

Abstract

In a systematic experimental study the behaviour of a periodically precessing jet is compared to that of the corresponding steady inline jet. The precessing motion is that of self-sustained unsteadiness which is a consequence of an axisymmetric "Coanda-like" effect. The flow field is characterised by mean flow, turbulence and frequency data from hot wire measurements. Heat transfer data in terms of Nusselt numbers are determined on a specially designed heat transfer plate in the plane of jet impingement.

1. Introduction

Convective heat transfer is one of the technically important modes of exchanging internal energy between a solid body and its ambient, either for cooling or heating the body. The rate of heat transfer in this process strongly depends on the flow field, its strength as well as its structure, with appropriate nondimensional heat transfer coefficients covering several orders of magnitude, when the flow field parameters are changed within reasonable ranges.

A standard situation in convective heat transfer is an impinging jet on a plane surface in an otherwise quiescent ambient. This arrangement is often used for body cooling. Due to the analogy of convective heat and mass transfer it is also important in drying processes.

Though the geometry of the jet/plate combination is quite simple there are nevertheless a large number of parameters in this convective heat transfer arrangement, like: nozzle to plate distance, *Re* number, turbulence level, nozzle inclination angle (if not vertical), wall roughness just to mention a few. All these parameters affect the heat transfer performance of the arrangement and can be changed systematically in order to influence the rate of heat transfer. The vast body of literature dealing with special aspects is well documented in review articles like [1–3].

Within the special means by which impinging jet heat transfer can be manipulated unsteadiness of the flow field is rarely used. However, unsteady flows are distinctly different compared to their steady counterparts, so that there should be a high potential to affect the heat transfer performance of such flows. Studies about the influence of unsteady flow fields on convective heat transfer almost always generate the unsteady flow by external means like forced pulsation or periodic interruption of the jet impingement. Typical studies of this kind are [4–7], with no general trend in the results: some find enhanced heat transfer, some don't.

Our approach, however, is a self-sustained unsteadiness without external input of energy and without moving parts in the system providing the flow field for convective heat transfer. There are "classical" ways to achieve this, like the famous von Karman vortex street behind a circular cylinder in cross flow or the flip-flop fluidic element (alternating flow in a Y-shaped conduct). A less well known configuration is that of a nozzle which due to its special design results in a periodically precessing jet. It is introduced with respect to its general

* Corresponding author. Tel.: +49-42-878-3044; fax: +49-42-878-4169.
E-mail address: h.herwig@tuhh.de (H. Herwig).

0017-9310/$ - see front matter © 2003 Elsevier Ltd. All rights reserved.
doi:10.1016/j.ijheatmasstransfer.2003.11.026

Nomenclature

A	surface
$\widehat{A}$	single field surface
D	diameter
f	frequency
h	nozzle height
H	nozzle/plate distance
k	thermal conductivity
Nu	Nusselt number, Eq. (1)
$\dot{q}$	heat flux density
R	electric resistence
Re	Reynolds number
Sr	Strouhal number
S	isolation material thickness
T	temperature
U	voltage
w	velocity
z_R	reference position
α	coefficient, Eq. (7)
ϵ	emissivity (total, hemispherical)
ν	kinematic viscosity
σ	Stefan–Boltzmann constant
Indices	
AMB	ambient
AS	air supply
c	conduction
e	electric
FC	flow control
HTS	heat transfer surface
i	isolation
IJN	inline jet nozzle
N	nozzle
PJN	precessing jet nozzle
r	radiation
rms	root mean square
R	reference
R	resistor
SF	single field
SF0	single field of temperature T_0
W	wall

performance at the beginning of Section 2 and in more detail later since it is the central part of our experimental set-up.

The objective of our study is to find out how strong convective heat transfer is influenced by the unsteady motion of the impinging jet, what are the crucial parameters of this configuration with respect to heat transfer and whether there is a potential for heat transfer augmentation. There are some aspects in favour of transfer augmentation like the fact that an unsteadily impinging jet results in a permanent boundary layer renewal. But there are also negative aspects like an increased mixing of the jet with the ambient fluid which reduces the jets maximum velocities and hence the good transfer properties of a narrow, high velocity jet. What is the overall effect is one of the questions that should be answered by our study.

2. Experimental apparatus and procedure

2.1. The precessing jet nozzle (PJN)

It is well known that a two-dimensional jet moves and finally sticks to an adjacent parallel wall due to pressure forces that are induced by the secondary entrainment flow at the edges of the jet. Once a wall is brought close to the jet the entrainment flow is restrained and a pressure lower than that on the other (unrestrained) side forces the jet to move towards the wall. This is known as Coanda effect. Even in a totally symmetrical situation like in Fig. 1a this happens after a slight perturbation has broken the symmetry. Since the symmetric flow field is unstable this slight unsymmetry is enhanced and finally moves the jet to one wall. Whether it is the left or the right wall depends on the initial perturbation.

Fig. 1b shows the same situation but now it is axisymmetric. Again the symmetrical flow case is unstable and a slight perturbation moves the jet toward the wall. However, now there is no left/right alternative. In

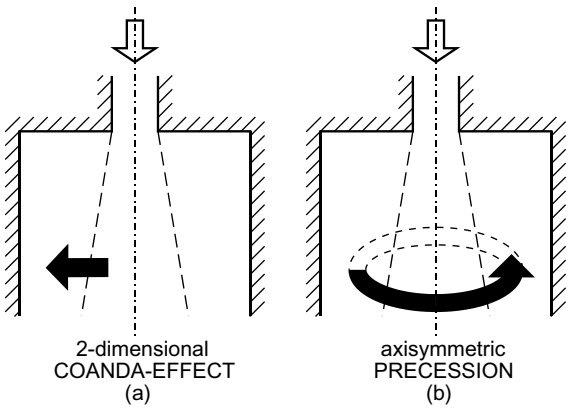

Fig. 1. 2D and axisymmetric jets under the influence of adjacent walls.

addition the perturbation will have an azimutal component forcing the jet (which moves towards the wall due to the radial perturbation) also to move azimutally, either in a left or a right turn, again depending on the initial perturbation. The final, stable flow field is that of a precessing jet, i.e. a jet that periodically moves along the inner wall with a fixed frequency. The jet axis is no longer in line with the symmetry line of the nozzle.

In a coordinate system fixed to the plate of the nozzle/plate configuration the flow from the nozzle impinges as a jet that periodically moves around an impingement circle. Thus, at a fixed point on the plate there is an unsteady (periodic) flow that will affect the convective heat transfer by this unsteadiness.

Due to the symmetry of this configuration the flow could alternatively be described as a steady flow if the coordinate system would move around with the jet. Then, however, the boundary condition at the heat transfer plate would be that of a moving wall. Since we want to address the question of how heat transfer at a (usually not moving) body can be controlled we definitely prefer a stationary coordinate system fixed to the wall in which the flow is clearly unsteady.

A similar nozzle has been incorporated in burners, see for example [9,10] with the aim of improving the mixing performance of these devices. As a first step we adopted the nozzle geometry of [8–10] with parameter values that are claimed to produce a stable periodic flow. This configuration is shown in Fig. 2a. However, in our experiments we only could achieve intermittent periodicity, i.e. periodical flows were interrupted stochastically by periods of steady axisymmetric flow. With certain core elements in the exit plane of the nozzle periodicity could be improved but still was not absolutely stable.

Fig. 2b shows our alternative which is not only easier to build but also has the property of a stable, uninterrupted precessing and thus unsteady flow. It simply consists of an additional *envelope tube* added to the nozzle opening of diameter D_1. However, it only works in a limited range of parameters D_2/D_1, h/D_2 and best with the parameter values given in the caption of Fig. 2.

2.2. The test facility

Fig. 3 is a schematic figure of our experimental design with the four main parts being the air supply, flow control, the nozzle and last but not least the heat transfer surface. All four will be described in detail hereafter. Also shown are the various data that are collected during the experiments and processed in our data acquisition system.

2.2.1. Air supply

The air was taken from the high pressure net in our lab. A pressure reduction valve including a filter together with a precision pressure control facility provided a constant air flow of adjustable rate.

In a flow meter the pressure difference Δp_{AS} across an orifice is measured and based on the calibration of the system the actual mass flux is determined. Electrical heating of the flow is installed in this section and controlled by temperature readings from the flow control part that is described next.

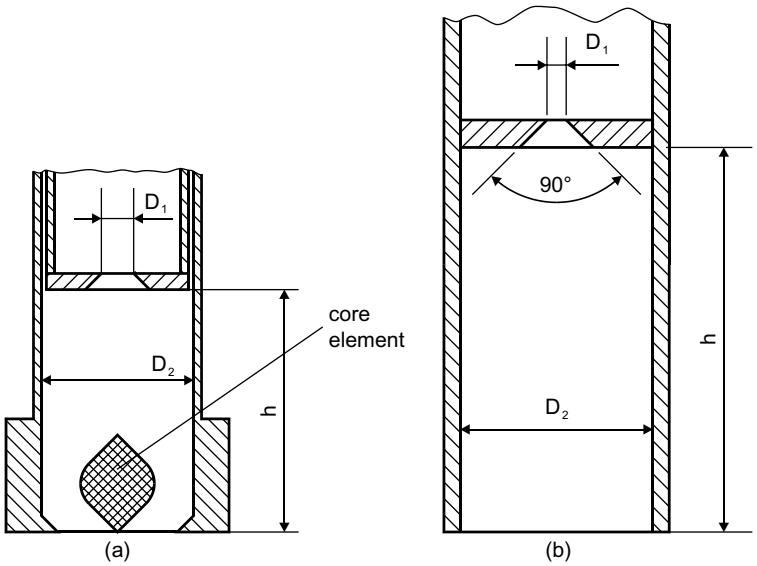

Fig. 2. Precessing jet nozzles (PJN). (a) PJN according to [8] recommended geometrical parameters: $\frac{D_2}{D_1} = 3.8–8$; $\frac{h}{D_2} = 2.7–3.5$, (b) PJN of our study: $\frac{D_2}{D_1} = 10$; $\frac{h}{D_2} = 2$.

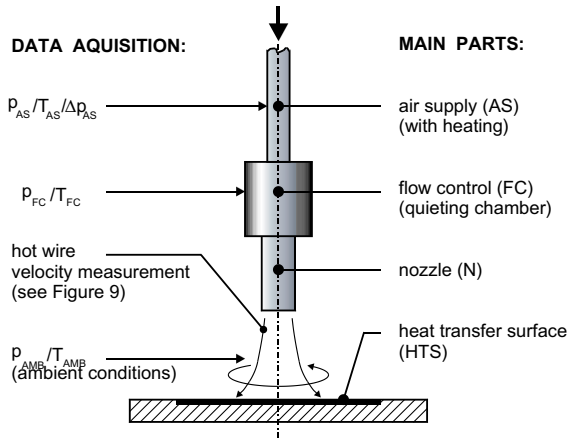

Fig. 3. Our test facility/main parts and data collected.

2.2.2. Flow control

Fig. 4 shows a quieting chamber which is the flow control part of our test facility. It provides a flow to the attached nozzle with

- a nearly uniform velocity profile
- a very low turbulence level
- a temperature T_{FC} equal to the ambient temperature T_{AMB}

The velocity and turbulence profiles in two perpendicular directions r_1 and r_2 shown in Fig. 4b are very uniform what we think is a necessary condition in order to test the performance of different nozzles. The influence of non-uniform influx conditions could differ from nozzle to nozzle spoiling the results.

Based on the temperature reading in the flow control chamber the electrical heating in the upstream air supply part is controlled in order to guarantee that T_{FC} is always equal to T_{AMB}. Thus, we avoid that heat transfer is affected by jet entrainment temperature effects.

2.2.3. Nozzle(s)

In Section 2.1 the design of the precessing jet nozzle (PJN) was described already. A crucial point in testing a new nozzle is the choice of an adequate reference case. After a careful consideration of all important aspects we decided to choose the inline jet nozzle (IJN) shown in Fig. 5 as our reference case. Thus, the only difference between the test and the reference nozzle is the additional envelope tube.

Comparison can and should be made at common numbers of the parameters which are the Reynolds number Re and the nozzle to plate distance H/D_1.

2.2.4. Heat transfer surface

From the rate by which an impinging jet cools a uniformly heated surface Nusselt numbers can easily be determined. Here the local Nusselt number Nu is defined as

$$Nu = \frac{\dot{q}_W D_1}{(T_W - T_{AMB})k} \tag{1}$$

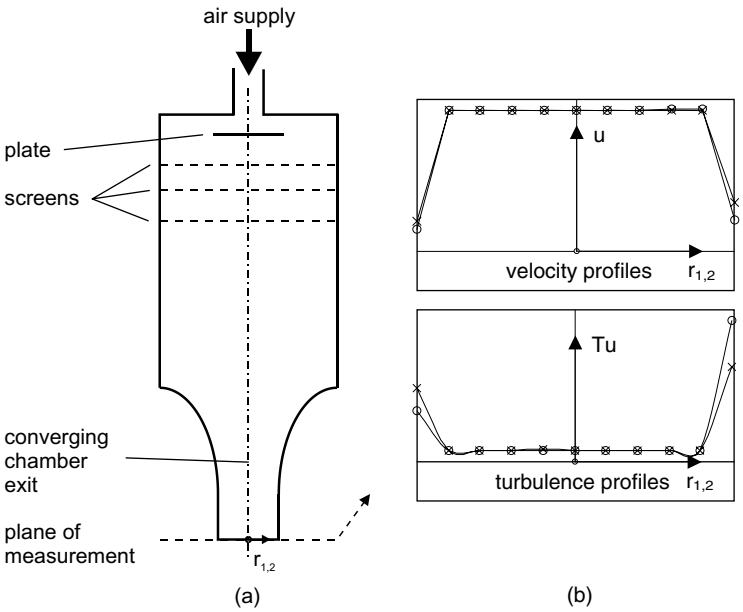

Fig. 4. Flow control in the quieting chamber. (ooo) profiles in r_1-direction, (xxx) profiles in r_2-direction.

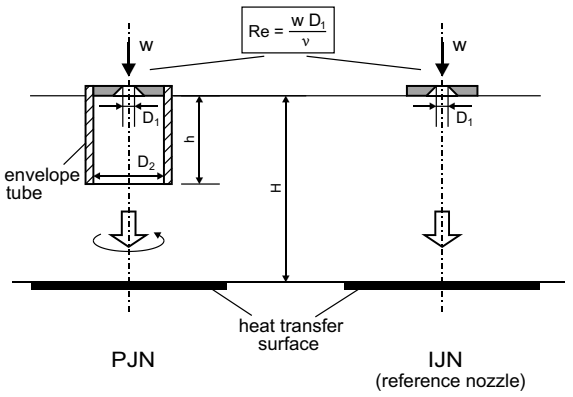

Fig. 5. The precessing jet nozzle (PJN) and its reference nozzle (IJN) arrangement. Common parameters are the Reynolds number Re and the nozzle to plate distance H/D_1.

with the local heat flux density at the wall ($\dot{q}_W$) and the local wall temperature (T_W).

Heat transfer coefficients with respect to finite parts $\widehat{A}$ of the surface are

$$\overline{Nu} = \frac{\bar{\dot{q}}_W D_1}{(\overline{T}_W - T_{AMB})k} \tag{2}$$

with $\bar{\dot{q}}_W = \frac{1}{\widehat{A}} \int \dot{q}_W \mathrm{d}A$ and $\overline{T}_W = \frac{1}{\widehat{A}} \int T_W \mathrm{d}A$ as surface averaged heat transfer density and temperature, respectively.

Fig. 6 sketches the design of our heat transfer plate for measuring wall heat flux densities and wall temperatures simultaneously. The main part of the heat transfer surface which has the double function of heating and measuring is an electrical circuit board with a special circuit design on both surfaces. The top surface which faces the impinging jet is covered with a densely meandering strip conductor between A and B. If there is uniform dissipation due to the electrical resistance of the conductor we thus get a local heat flux density at the wall which is almost constant (on a scale larger than the distance between two conductors). The central part of the plate is subdivided into 64 single fields of size (46.8 mm)^2 so that the whole heat transfer surface covers an area of (374.4 mm)^2. The grey shaded part around this surface in Fig. 6 is for additional heating in order to reduce the heat losses towards the edges of our heat transfer plate.

For each of the 64 single fields the voltage can be measured between contacts that are led through the plate and continued to the edge of it on the rear part (bottom surface) of the board by appropriate strip conductors.

If now the board is heated with a constant electrical current (typical value: 4 A) we measure the electrical current by determining the voltage U_R across a resistor of $R_R \approx 4\ \Omega$ and the single field voltage U_{SF}. When the whole arrangement is calibrated with respect to its temperature/electrical resistance behaviour (i.e. $R_{SF}(T)$ is known for each of the 64 single fields; R_{SF}: single field resistance, T: temperature) we find the electrical power density of a single field as

$$\dot{q}_{SF,e} = \frac{U_{SF}(U_R/R_R)}{\widehat{A}_{SF}} \tag{3}$$

From this we get the wall heat flux density $\bar{\dot{q}}_W$ in Eq. (2) for a single field by taking into account the additional radiation flux density

$$\bar{\dot{q}}_{SF,r} = \varepsilon\sigma(\overline{T}_W^4 - T_{AMB}^4) \tag{4}$$

and losses by heat conduction to the rear of our heat transfer plate. With isolation foam material of thickness S_i and conductivity k_i they can be kept small and are

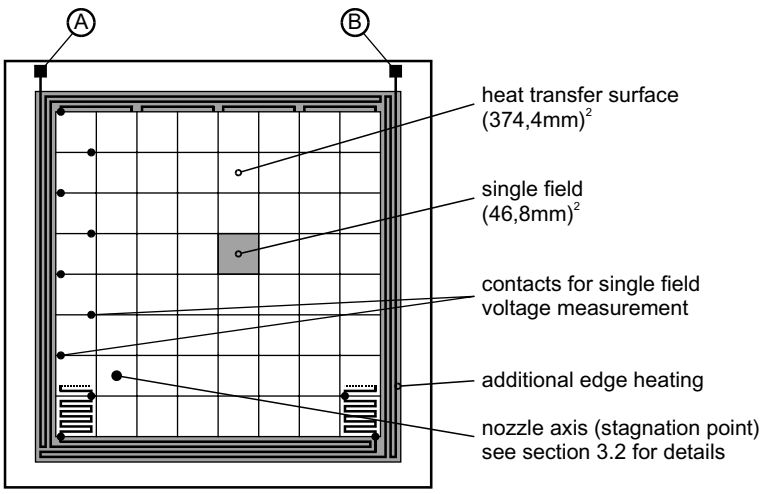

Fig. 6. Details of the heat transfer plate.

$$\bar{\dot{q}}_{\mathrm{SF,c}} = k_i \frac{(\Delta T)_i}{S_i} \tag{5}$$

where $(\Delta T)_i$ is the temperature difference across the isolation material.

Thus we get for $\bar{\dot{q}}_{\mathrm{W}}$, the heat flux density of a single field in Eq. (2):

$$\bar{\dot{q}}_{\mathrm{W}} = \bar{\dot{q}}_{\mathrm{SF,e}} - \bar{\dot{q}}_{\mathrm{SF,r}} - \bar{\dot{q}}_{\mathrm{SF,c}} \tag{6}$$

The single field temperature $\overline{T}_{\mathrm{W}}$ can be determined as soon as the $R_{\mathrm{SF}}(T)$ relation is known through a calibration process. For small temperature differences (like in our case) the linear function $R_{\mathrm{SF}}(T) = R_{\mathrm{SF0}}[1+\alpha_{\mathrm{SF}}(T-T_0)]$ is sufficient, so that $\overline{T}_{\mathrm{W}}$ in Eq. (2) is found as

$$\overline{T}_{\mathrm{W}} = T_0 + \frac{R_{\mathrm{SF}} - R_{\mathrm{SF0}}}{\alpha_{\mathrm{SF}} R_{\mathrm{SF0}}} \quad \text{with} \quad R_{\mathrm{SF}} = R_{\mathrm{R}} \frac{U_{\mathrm{SF}}}{U_{\mathrm{R}}} \tag{7}$$

By calibrating the heat transfer plate the single field coefficients α_{SF} and R_{SF0} are determined. The coefficients α_{SF} differ by less than 0.2% between the 64 single fields.

So far only single field averaged quantities can be determined and the Nusselt number will be $\overline{N}u_{\mathrm{SF}}$ according to Eq. (2), i.e. an averaged Nusselt number for each of the 64 single fields. In order to get local values of the Nusselt number we prepared the heat transfer surface for infrared temperature measurements by coating them with black mat paint. Assuming $\dot{q}_{\mathrm{W}}$ to be sufficiently constant across the heat transfer surface local temperature measurements by IR technique thus can give local Nusselt numbers according to Eq. (1).

3. Experimental results

Since in forced convective heat transfer there is a strong influence of the flow field on the temperature field (and thus on the heat transfer rate at the wall) but no or only a minor influence the other way round, we first analysed the flow field of the PJN above a heat transfer surface and then its impact on the heat transfer performance of a PJN/plate arrangement.

The crucial parameters of our nozzle/plate configuration are

- Reynolds number $Re = wD_1/\nu$; see Fig. 5
- nozzle to plate distance H/D_1; see Fig. 5
- Strouhal number $Sr = fD_1/w$ of the precessing flow field

When the Reynolds number and the nozzle to plate distance are fixed there is no longer a free choice with respect to the Strouhal number, since the precession frequency f is an inherent feature of the unsteady flow field. Only when D_1 is changed, different Sr numbers exist for the same values of Re and H/D_1. This is why we performed our experiments with two different nozzles, one with $D_1 = 3.5$ mm and one with $D_1 = 5$ mm.

3.1. Flow field characteristics

Prior to looking at details of the flow field the overall performance of the PJN was tested in terms of power that is needed for the flow to exist and which is dissipated completely in the flow field. Therefore it is called P_{LOSS}. This power has to overcome the pressure difference $(p_{\mathrm{AMB}} - p_{\mathrm{FC}})$ and provide the kinetic energy in the quieting chamber where the mean velocity is w_{FC}. With a volume flow rate $\dot{V}_{\mathrm{FC}}$ which can be determined from our mass flux measurements in the air supply part, we get

$$P_{\mathrm{LOSS}} = \dot{V}_{\mathrm{FC}}\left[(p_{\mathrm{FC}} - p_{\mathrm{AMB}}) + \frac{\rho_{\mathrm{FC}}}{2} w_{\mathrm{FC}}^2\right] \tag{8}$$

There is almost no difference between IJN and PJN which means that only a very small upstream influence exists that might feed back the totally different flow field behaviour once the flow has passed through the D_1 cross section.

For incompressible flow there would be a $P_{\mathrm{LOSS}} \sim Re^3$ dependence. Since, however, nozzle exit velocities are very high (s. Table 2 in Section 3.2) this can only be found for the low Reynolds numbers.

Though P_{LOSS} for the IJN and PJN arrangements are virtually the same the flow field downstream of the D_1 cross section is completely different. Fig. 7 shows time averaged velocity profiles for both cases from hot wire measurements. For the steady IJN case this is the standard representation of a turbulent velocity profile. The unsteady PJN case, however, is best represented by conditional sampling with a phase locked trigger mechanism which could separate the unsteady (low frequency) part from the turbulent (high frequency) behaviour. In our case, however, the periodicity of the precessing motion was not stable enough for such a kind of data processing. Therefore, we also time-averaged the unsteady turbulent motion in the conventional way and at this stage thus cannot tell periodic from turbulent contributions to the final velocity profiles.

In most cases the velocity profiles turned out to be sufficiently symmetrical so that they can be displayed by showing just one half of each profile with corresponding IJN and PJN cases facing each other like in Fig. 7. Since $z_{\mathrm{R}}/D_1 = 20$ for the PJN-case is the end of the envelope tube, the velocity profile is very special there. Further downstream IJN and PJN profiles are not fundamentally different but PJN profiles are far wider spread than in-line profiles.

In Fig. 8 the same z-dependent velocity u_{R}, i.e. $\bar{u}$ at $x = 0$, $z = z_{\mathrm{R}}$, is used to nondimensionalize the u_{rms} values of u. Thus, ratio $u_{\mathrm{rms}}/u_{\mathrm{R}}$ directly shows how velocity fluctuations vary with radial distance. This ratio from our point of view is a better representation of

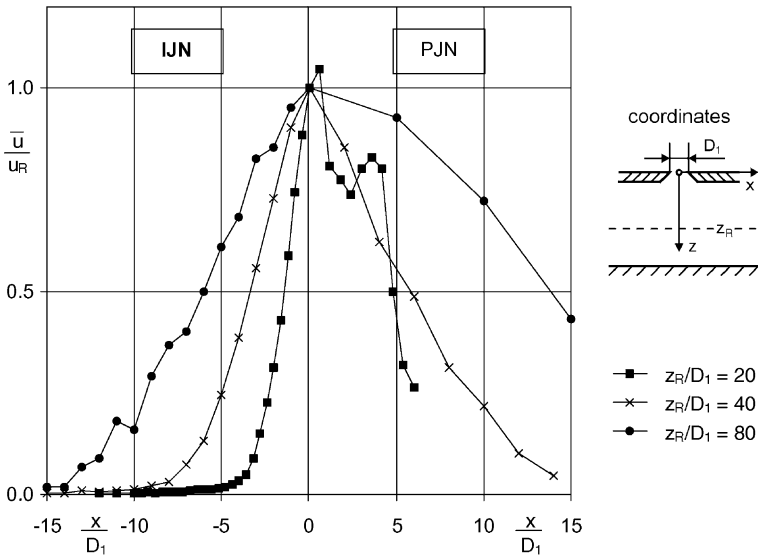

Fig. 7. Comparing dimensionless velocity profiles $\bar{u}/u_R$. Here u_R: velocity $\bar{u}$ at $x = 0$, $z = z_R$; $D_1 = 5$ mm.

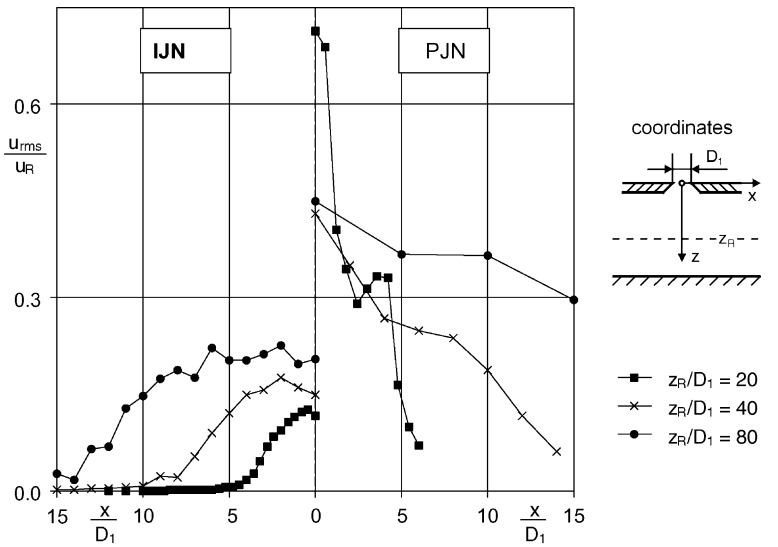

Fig. 8. Comparing turbulence intensity profiles u_{rms}/u_R. Here u_R: velocity $\bar{u}$ at $x = 0$, $z = z_R$; $D_1 = 5$ mm.

turbulence intensity than an intensity defined with the local (i.e. z and x dependent) reference velocity that is often used. Again the PJN profiles are spread much wider.

In Table 1 the numbers of u_R are given for the profiles shown in Figs. 7 and 8 so that absolute values for $\bar{u}$ and u_{rms} can be determined in the figures through the products $(\bar{u}/u_R)u_R$ and $(u_{rms}/u_R)u_R$, respectively.

To summarise the flow field results given so far: Though P_{LOSS} is almost the same in both cases the flow fields differ substantially in terms of much wider spread profiles.

Table 1
Reference velocities at three different downstream positions

z_R/D_1	u_R (IJN) (m/s)	u_R (PJN) (m/s)
20	65.4	17.9
40	30.9	11.8
80	16.4	4.6

Since unsteadiness and turbulence are not accounted for separately in the averaging process used so far, we next determined the Strouhal number of the PJN arrangement which may be regarded as the crucial

parameter that characterises our periodically unsteady flow field.

Fig. 9 shows the typical time periodic behaviour of the flow field, here in terms of the u-velocity component measured by hot wire anemometry at a position in the flow field marked in Fig. 3. From a spectral analysis of this signal the precession frequency can be easily identified. This frequency increases with the flow rate (Re number). For the example shown, the frequency range is about 10–30 Hz which is a typical range for PJN arrangements of our study.

The range of Strouhal numbers

$$Sr = \frac{fD_1}{w} \tag{9}$$

in Fig. 10 is $7.7 < 10^4 Sr < 9.9$ with Reynolds numbers $Re = wD_1/v$ between 26 000 and 145 700.

3.2. Heat transfer results

Nusselt numbers and Nusselt number distributions were determined on the heat transfer surface described in Section 2.2. After we made sure that the heat transfer distribution is sufficiently rotationally symmetrical with the nozzle axis in the midpoint of the square surface we

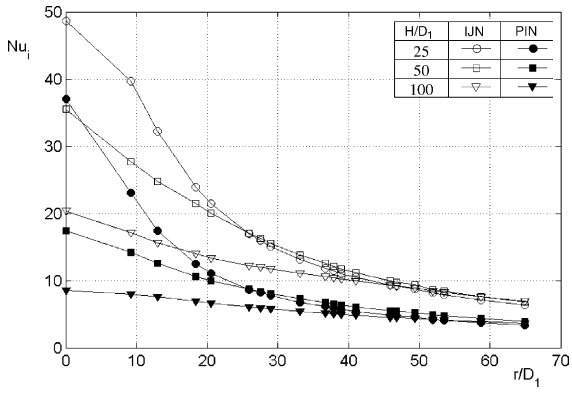

Fig. 10. Heat transfer PJN ($D_1 = 5$ mm) versus IJN Nusselt numbers $\overline{N}u_i$ for the single fields as quasi-radial Nusselt number distribution on the heat transfer surface $Re = 5.8 \times 10^4$.

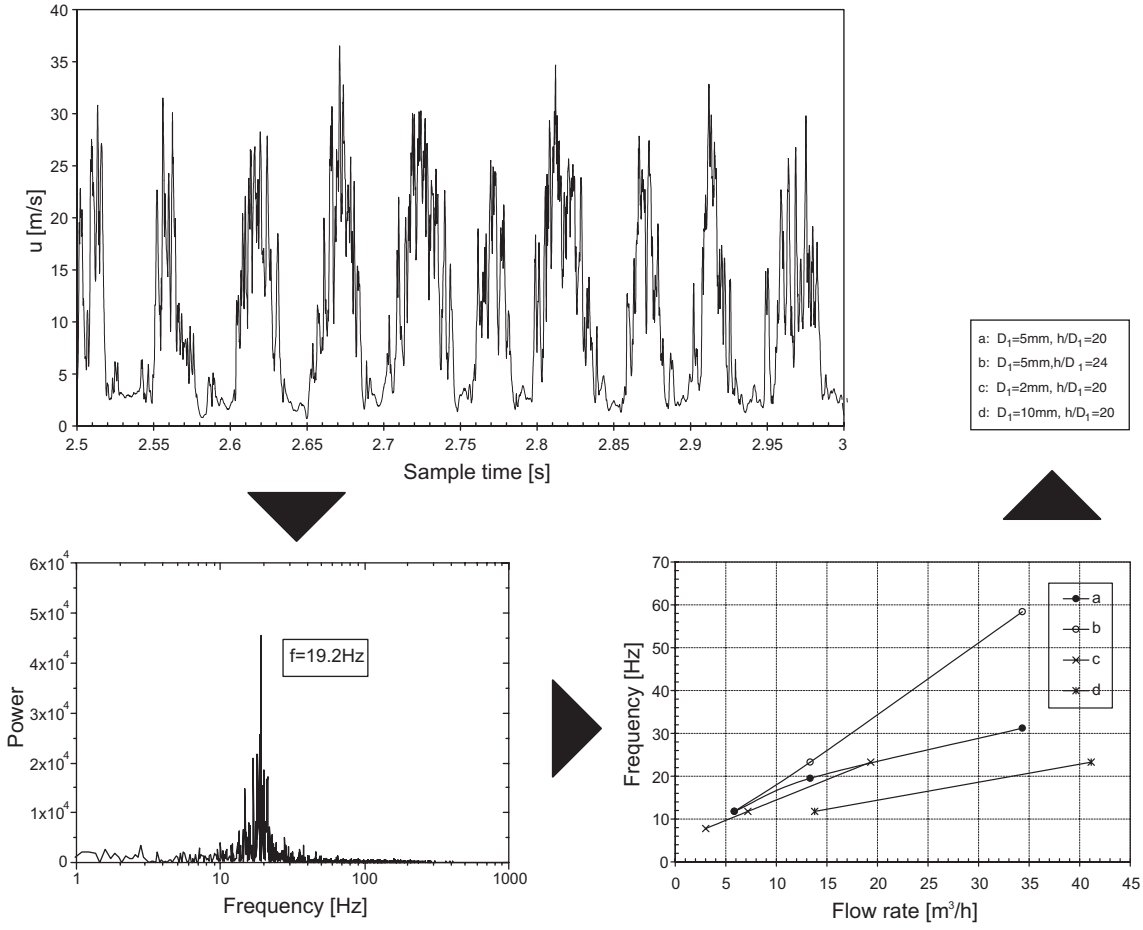

Fig. 9. Velocity signal, power spectrum and precession frequency for a typical PJN arrangement; $D_1 = 5$ mm.

placed the jet axis off midpoint in a position shown in Fig. 6. We thus get results for larger radii.

For each of the single fields we get one Nusselt number averaged over the single field area ((46.8 mm)^2). With corresponding fields (located symmetrically with respect to the diagonal) combined to an (arithmetic) mean value we thus get 20 Nusselt numbers for fields located at different distances from the stagnation point. Plotted as $\overline{Nu}_i$ over r/D_1 (with $0 \leqslant r/D_1 \leqslant 66$ for $D_1 = 5$ mm and $0 \leqslant r/D_1 \leqslant 95$ for $D_1 = 3.5$ mm) we get the quasi-radial distribution of the Nusselt number under the impinging jets. The term "quasi-radial" refers to the fact that our Nusselt numbers (so far) are not measured locally, but averaged over small single fields of the whole heat transfer surface.

In Table 2 the whole measuring program is listed for both nozzles ($D_1 = 5$ mm, $D_1 = 3.5$ mm). Those results that are shown and discussed in the subsequent Figs. 10–12 are marked. For all PJN flows in Table 2 corresponding IJN flows have been measured (with a mass flux $\dot{m}$, velocity w and Reynolds number Re being the same within measuring uncertainties, see Section 3.4).

Figs. 10 and 11 show Nusselt number distributions for three nozzle to plate distances for the precessing jets (PJN) and the corresponding inline jets (IJN). It turns out that in all cases shown as well as in all cases in Table 2 which are not shown explicitly Nusselt numbers for the PJN arrangement are below those for the corresponding inline jets. Obviously the increased mixing of the jet with the ambient fluid dominates the heat transfer behaviour

Table 2
Precessing jet results for two different nozzles

H/D_1	$\dot{m}$/kg/s	w/m/s	P_{LOSS}/W	f/Hz	Sr	Re	
$D_1 = 5$ mm ($D_2/D_1 = 10$; $h/D_1 = 20$)							
25							
50	1.9×10^{-3}	76.7	11.9	11.8	7.7×10^{-4}	2.6×10^{4}	
100							
25							
50	2.8×10^{-3}	107	34.4	15.8	7.4×10^{-4}	3.9×10^{4}	
100							
25							
50	4.2×10^{-3}	141	93.1	23.3	8.3×10^{-4}	5.8×10^{4}	◀ Fig. 10
100							
25							
50	6.3×10^{-3}	169	234	35.1	10.4×10^{-4}	8.9×10^{4}	
100							
25							
50	1.1×10^{-2}	204	577	38.7	9.5×10^{-4}	16×10^{4}	
100							
$D_1 = 3.5$ mm ($D_2/D_1 = 10; h/D_1 = 20$)							
25							
50	1.2×10^{-3}	106	11.6	17.7	5.8×10^{-4}	2.4×10^{4}	
100							
25							
50	1.8×10^{-3}	146	31.8	22.5	5.4×10^{-4}	3.7×10^{4}	
100							
25							
50	2.7×10^{-3}	194	80.9	30.2	5.4×10^{-4}	5.6×10^{4}	◀ Fig. 11
100							
25							
50	4.2×10^{-3}	241	189	44.9	6.5×10^{-4}	8.9×10^{4}	
100							
25							
50	6.8×10^{-3}	259	407	73.0	9.9×10^{-4}	14.6×10^{4}	◀ Fig. 12
100							

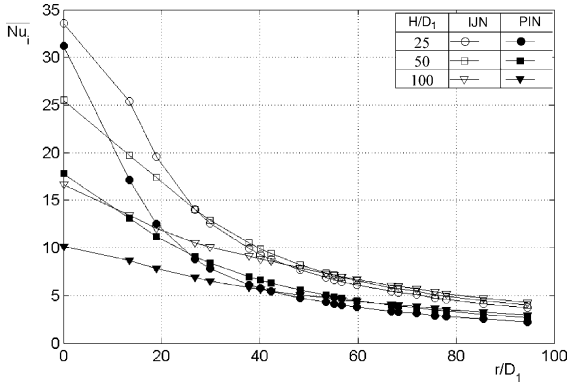

Fig. 11. Heat transfer PJN ($D_1 = 3.5$ mm) versus IJN Nusselt numbers $\overline{Nu}_i$ for the single fields as quasi-radial Nusselt number distribution on the heat transfer surface $Re = 5.6 \times 10^4$.

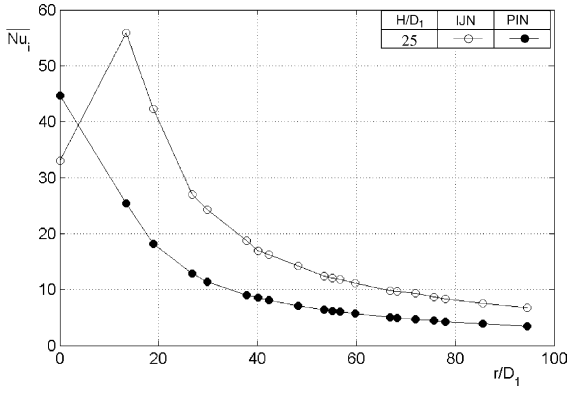

Fig. 12. Heat transfer PJN ($D_1 = 3.5$ mm) versus IJN $Re = 14.6 \times 10^4$; $f = 73$ Hz.

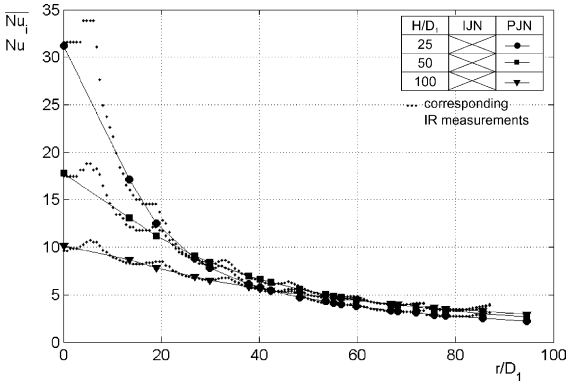

Fig. 13. Infrared measurements compared to the single field electrical measurements used in all previous figures. $D_1 = 3.5$ mm; $Re = 5.6 \times 10^4$; PJN (see Fig. 11).

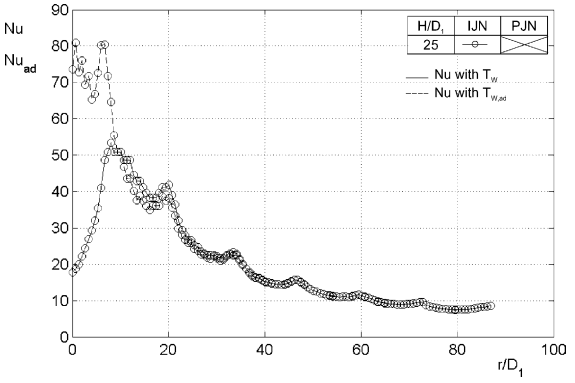

Fig. 14. Heat transfer IJN ($D_1 = 3.5$) $Re = 14.6 \times 10^4$ (see Fig. 12).

by overriding the potential heat transfer enhancement through unsteady boundary layer renewal.

This is true even for higher precession frequencies as can be seen from Fig. 12. Here for $H/D_1 = 25$ PJN and IJN results are shown in a situation where the precession frequency is increased to $f = 73$ Hz compared to $f = 23$ and $f = 30$ in Figs. 10 and 11 respectively. Why there is a very low Nusselt number at the stagnation point for the inline jet will be explained in the next section (Fig. 14).

3.3. Special aspects

Since we coated our heat transfer surface with black mat paint infrared (IR) measurements are possible to achieve real local Nusselt number distributions. Fig. 13 shows such a measurement along the diagonal of our heat transfer surface. The single field structure can clearly be identified in the Nusselt number distribution, since obviously the assumed $\dot{q}_W = \text{const.}$ heating is not perfectly realised at the edges of the single fields. Nevertheless there is a good coincidence of single field ($\overline{Nu_i}$) and IR (Nu) data.

At least for those cases with high Reynolds numbers there will be considerable viscous heating on the surface which should be taken into account. An appropriate way is to use the adiabatic wall temperature $T_{W,ad}$ instead of the wall temperature T_W in the definition of Nu, see Eq. (1). Fig. 14 shows that Nu compared to Nu_{ad} is substantially different in the vicinity of the stagnation point for inline jets at very high Reynolds numbers. However, for moderate Reynolds numbers and away from the stagnation region the difference is only marginal.

3.4. Error analysis

In a detailed error analysis we identified and evaluated all elements of the "measuring chain" that influence

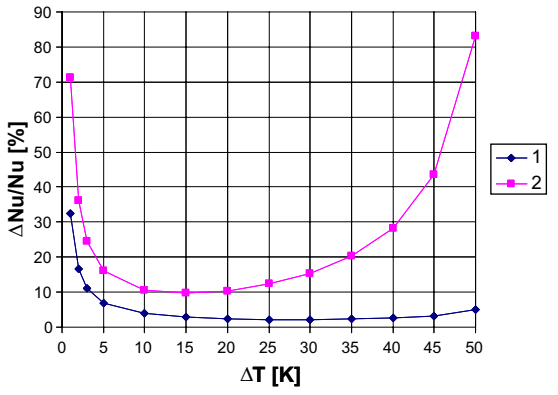

Fig. 15. Nusselt number uncertainties. Curve 1: relative uncertainty (no systematic errors), curve 2: absolute uncertainty.

the accuracy of our Nusselt number results. Based on this detailed analysis we end up with the uncertainty

$$\frac{\Delta Nu}{Nu} = \left|\frac{\Delta \dot{q}_W}{\dot{q}_W}\right| + \left|\frac{\Delta T_W}{T_W - T_{AMB}}\right| + \left|\frac{\Delta T_{AMB}}{T_W - T_{AMB}}\right| \quad (10)$$

assuming that D_1 and k do not contribute to $\Delta Nu/Nu$.

In Fig. 15 the relative as well as the absolute uncertainties are shown for our measurements of the Nusselt numbers. Curve 1 for the relative uncertainty neglects all systematic errors and is the relevant curve when certain parameters are changed in an otherwise unchanged setting as was the case in our Figs. 10–14 for example. Curve 2 includes all systematic errors and is an upper bound when it comes to a comparison with results from other studies that use different measuring techniques (but with systematic errors that do not exceed our ones).

Similar considerations with respect to the Reynolds number reveal a 3% uncertainty for that quantity.

From these results we conclude that our experimental set-up provided data of sufficient accuracy to come to the conclusions we summarise in the following section.

4. Discussion

As a result of our study three main conclusions can be drawn that might be important for all those who plan to incorporate unsteady jet impingement in heat and/or mass transfer processes

- A stable self-sustained periodic flow can be achieved by very simple means with no need for external energy or moving parts. It is characterised by an almost constant Strouhal number even for a wide range of geometry and flow parameters.
- The flow field with and without unsteady motion is substantially different; the pressure drop across the corresponding nozzles, however, is not. Velocity profiles in the unsteady case show strong mixing of the jet with ambient fluid and thus a rapid decrease in the maximum jet velocity.
- Due to the rapid mixing with ambient fluid convection velocities at the heat transfer surface are relatively small and thus lead to a reduction in heat transfer. This can be stated as a general trend though the margins of reduction depend on various parameters.

Since there are arguments "pro and con" positive effects of unsteadiness with respect to a heat transfer augmentation it was not clear in the beginning, if the precessing jet might be used for that purpose. However, it turned out that the negative effect of mixing obviously overwhelms the positive effect of a permanent boundary layer renewal at the heat transfer surface.

From other studies about unsteady heat transfer it is known that there often is a threshold-frequency above which augmentation occurs. In our study, however, there was no clear trend towards an augmentation with increasing precessing frequency.

If at all, it might occur at frequencies which are at least an order of magnitude higher. This, however, was beyond the range of parameters that we could realise in our experimental set-up.

Acknowledgements

The authors would like to thank the DFG (Deutsche Forschungsgemeinschaft) for the support of this study.

References

[1] H. Martin, Heat and mass transfer between impinging gas jets and solid surfaces, Adv. Heat Transfer 13 (1977) 1–60.
[2] K. Jambunathan et al., A review of heat transfer data for single circular jet impingement, Int. J. Heat Fluid Flow 13 (2) (1992) 106–115.
[3] R. Viskanta, Heat transfer to impinging isothermal gas and flame jets, Exp. Thermal Fluid Sci. 6 (1993) 111–134.
[4] D.A. Zumbrunnen, M. Aziz, Convective heat transfer enhancement due to intermittency in an impinging jet, J. Heat Transfer 115 (1993) 91–98.
[5] L.F.A. Azevedo, B.W. Webb, M. Queiroz, Pulsed air jet impingement heat transfer, Exp. Thermal Fluid Sci. 8 (1994) 206–213.
[6] E.C. Mladin, D.A. Zumbrunnen, Local Convective Heat Transfer to Submerged Pulsating Jets, Int. J. Heat Mass Transfer 40 (14) (1997) 3305–3321.

[7] T. Liu, J.P. Sullivan, Heat transfer and flow structures in an excited circular impinging jet, Int. J. Heat Mass Transfer 39 (17) (1996) 3695–3706.
[8] G.J. Nathan, The enhanced mixing burner, PhD Thesis, Department of Mechanical Engineering, The University of Adelaide, 1988.
[9] G.J. Nathan, R.E. Luxton, Mixing enhancement by a self-exciting, axisymmetric precessing flow-field, in: 4th International Symposium of Transport Phenomena, Sydney, Australia, 1991.
[10] G.J. Nathan, R.E. Luxton, J.P. Smart, Reduced NO_x emissions and enhanced large scale turbulence from a precessing jet burner, in: 24th Symposium (International) on Combustion, The Combustion Institute, Sydney, Australia, 1992.